processes

MDPI

*Article*

# Characteristic Analysis of Finite Dissipation Zone in Directional Material Flow

**Hong Ren [1,2,*], Wenjun Meng [1,2,*], Xiaoxia Sun [1,2,3], Zhangda Zhao [1,2] and Xiaoxia Zhao [1,2]**

[1] School of Mechanical Engineering, Taiyuan University of Science and Technology, Taiyuan 030024, China; 2005053@tyust.edu.cn (X.S.); zhaolei678@foxmail.com (Z.Z.); morningdian@163.com (X.Z.)
[2] Shanxi Key Laboratory of Intelligent Logistics Equipment, Taiyuan 030024, China
[3] Department of Engineering, School of International Studies, Krirk University, Bangkok 10220, Thailand
* Correspondence: tyustrh@stu.tyust.edu.cn (H.R.); tyustmwj@126.com (W.M.); Tel.: +86-0351-6998115 (H.R. & W.M.)

**Abstract:** Materials compress each other in a directional material flow, causing energy and momentum to overflow. Materials moving at a low velocity outside the boundary of a rigid moving component form a finite dissipation zone. A discrete element model is established to explore its characteristics. First, the mass of material driven by the disk increases linearly with an increase in the translation distance, and the mass of material moving at a low velocity increases significantly. Second, the movement state of materials depends on its distance from the disk. The material velocity at the boundary of the finite dissipation zone is verified to be 1 mm/s by analyzing the material velocity and contact force. When the operating parameters are different, the boundary curves of the finite dissipation zone are similar but the numerical values are different. Third, the maximum edge extends 0.7–3.0 mm beyond the boundary, and this value is linearly related to the translation velocity with little impact from the lowering depth. Studying the mechanism of finite dissipation zones contributes to forming an efficient directional material flow and the energy dissipation mechanism under a flexible constraint.

**Keywords:** DEM; directional material flow; finite dissipation zone; material movement



**Citation:** Ren, H.; Meng, W.; Sun, X.; Zhao, Z.; Zhao, X. Characteristic Analysis of Finite Dissipation Zone in Directional Material Flow. *Processes* **2023**, *11*, 1670. https://doi.org/10.3390/pr11061670

Academic Editor: Alberto Di Renzo

Received: 26 April 2023
Revised: 29 May 2023
Accepted: 30 May 2023
Published: 31 May 2023



## 1. Introduction

Relying on gravity to spread/discharge materials in large flat-bottomed silos causes problems, such as materials accumulating into hills and large amounts of residual materials being produced during discharging, which reduce the effective capacity and utilization efficiency of the silo. Therefore, flat-bottom silos are equipped with spreading/discharging devices that produce directional material flow on the surface of the material to achieve controllable and efficient spreading and discharging within the silo [1–3].

The projection of a screw blade is circular in the axial direction. The screw enters the material surface to a certain depth and then it rotates to promote the movement of the material along the axis direction, creating a directional material flow [4,5]. However, a horizontal trough-free screw lacks a rigid and smooth trough during spreading. The tight contact between stationary and moving materials causes the screw action to overflow, as shown in Figure 1. Additionally, the scope of action of the screw is not limited to the diameter of the screw blade. The energy is absorbed by the material outside the diameter of the screw blade during the movement of the material driven by the screw, forming a rough constraint surface with a certain thickness (and an assumed equivalent value of $\Delta R$) around the boundary of the screw blade. This is known as a finite dissipation zone, whose characteristics change with variations in the operating parameters.

In addition to a finite dissipation zone outside the screw, there is strong contact and compression between the stationary and moving materials when there is no rigid trough outside the moving material. This creates a gradient transfer of energy and momentum that

requires a finite dissipation zone [6,7]. This study uses a disk instead of a screw blade to simplify the research object, which can be moved along the axis of the disk after reaching a certain depth on the surface of the material. The proposed disk also achieved a directional material flow, which was used to study the relevant characteristics of the finite dissipation zone and reduce the required computational domain.

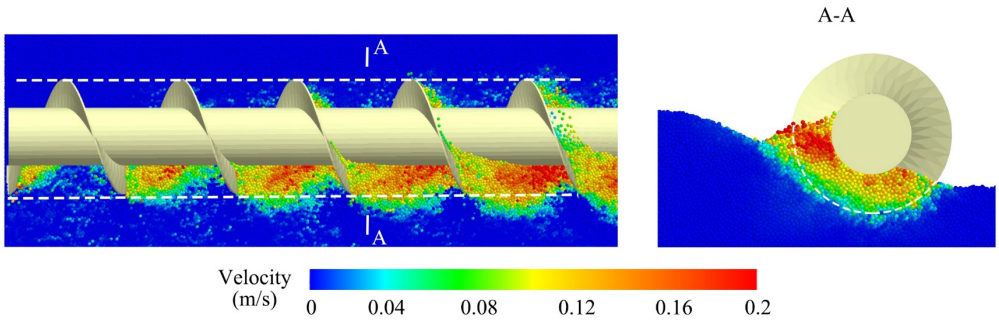


**Figure 1.** There is material outside the diameter of the screw that moves under the screw's action. The dashed line represents the boundary of the screw and the right figure shows the cross-sectional view at section A-A in the left figure.

A finite dissipation zone is mainly used to study the motion states of materials below the surface. Visual detection methods, such as particle image velocimetry, particle tracking velocimetry, and digital image correlation, can only observe the motion state of surface materials in dense particle flows and cannot be used to study the characteristics of a limited dissipation zone. X-ray and nuclear magnetic resonance can penetrate the interior of materials; however, they are expensive and complex experimental methods that are generally used for quasi-static flows. Additionally, the number of tracked particles is relatively low, making it difficult to detect the particle flow. There are almost no effective means of performing dynamic measurements [8–12]. The Discrete Element Method (DEM) has been effectively used to predict and analyze the behavior, state, and stress of materials [13–15]. Sadek used the DEM to predict changes in the resistance of a disk plough when the tillage depth, tillage speed, and disk diameter were varied [16]. It was found that the tillage depth and speed had significant impacts on the resistance, whereas the resistance was almost unchanged when the diameter varied between 457 and 660 mm. Coetzee studied the change rule of the material shear surface during the passage of a flat plate into a certain depth of material and found that the shear surface was not an inclined surface [17]. Instead, the shear surface was at a certain distance from the edge of the flat plate to a greater depth and then tilted to reach the material surface. Both of the abovementioned studies focused on the changes in the operating parameters that caused material movement outside the edges of the moving components. However, the characteristics of the finite dissipation zone have not been thoroughly studied. Zhang investigated the law of force transfer in regularly arranged particles using a diamond grid [18]. It was found that a single point of force transfer between materials formed a gradually decreasing network. Additionally, there was a decreasing force network between materials outside the disk boundary, resulting in gradient differences in physical quantities, such as displacement and energy.

Materials within the diameter of a disk receive a continuous energy input from the disk, and materials outside the edge move slowly through contact between materials driven by the friction of the moving materials, expanding the range of action of the disk. Materials in a finite dissipation zone are essentially unable to obtain a continuous energy input and thus stop after a short period of movement, ultimately dissipating the input energy. The movement state of the materials in a finite dissipation zone is the key point of this study. Understanding the mechanisms and characteristics of the composition of the movement state can determine its location and size, reduce energy dissipation, and positively affect the efficient directional flow of materials.

The DEM was used to systematically simulate the directional material flow driven by an external force. The characteristics and mechanisms of the finite dissipation zone under different operating parameters were studied by combining criteria, such as the material velocity, displacement, and contact force. The amount of moving material gradually increased as the disk continued to move. Furthermore, the amount of material in the finite dissipation zone increased significantly. It was determined that the velocity of the materials at the boundary was 1 mm/s during the stable state by analyzing the displacement of the materials in the finite dissipation zone. This was verified by the variation in the velocity and contact force of the materials inside and outside the finite dissipation zone. The maximum edge of the finite dissipation zone extended from 0.7–3.0 mm beyond the boundary, and its value was linearly related to the translational velocity, with little influence from the lowering depth. The angle from the edge of the disk to the maximum edge of the finite dissipation zone was almost constant during the disk-pushing stage. Increases in the amount of material in the finite dissipation zone caused changes in the slope and length of the finite dissipation zone after the maximum edge, thereby increasing the area of the finite dissipation zone. The laws of force and energy overflow in a finite dissipation zone were obtained in this study, and the conclusions can be used to optimize the operating parameters and facilitate the formation of efficient and green directional material flows.

## 2. Simulation Methods

### 2.1. Energy and Material Movement

The movement of materials driven by a disk is a process of continuous energy exchange. The material system is an energy dissipation system. The external energy input is dissipated through friction and inelastic collisions, and the remainder is converted into kinetic or potential energy. A bulk material system requires a constant input of external energy to maintain its stable state.

According to the kinetic energy theorem and law of conservation of energy, the energy input by the disk is converted into the kinetic, potential, and dissipated energies of the material, which is expressed as:

$$\Delta E_k = E_{k1} - E_{k0} = W_s - \Delta E_p - E_f \tag{1}$$

where $\Delta E_k$ denotes the change in kinetic energy, $W_s$ denotes the work of the disk, $\Delta E_p$ denotes the change in potential energy, and $E_f$ denotes the energy consumed during material movement. Subscripts 0 and 1 represent the beginning and end times, respectively.

$E_p$ can be divided into gravitational and elastic potential energies ($E_T$). $E_T$ is the energy stored after the material is deformed by the contact force. $E_k$ is the kinetic energy of the particle translation and rotation [19]. The equations used in this study are expressed as:

$$\begin{aligned} E_k &= \sum_1^N \left( \tfrac{1}{2} m_p v_p^2 + \tfrac{1}{2} I_p {\omega_p}^2 \right) \\ E_p &= \sum_1^N m_p g \triangle h_p + E_T \end{aligned} \tag{2}$$

where $m_p$ and $v_p$ denote the mass and translational velocity of a single particle, respectively. $I_p$ and $\omega_p$ denote the moment of inertia and rotational speed of a single particle, respectively. $\Delta h_p$ denotes the height change of the material, $E_T$ denotes the elastic potential energy, and $N$ denotes the number of material particles [20].

The elastic potential energy of a single particle is equal to the work performed by the normal contact force ($F_{c,n}$) between the particles from the contact starting point to the endpoint [5]. The elastic potential energy is expressed as:

$$E_T \approx \sum_1^N \sum_1^{k_p} \frac{2}{5} \left( \frac{4}{3} E^* \sqrt{R^*} \right)^{\frac{2}{3}} {F_{c,n}}^{\frac{5}{3}} \tag{3}$$

where $F_{c,n}$ denotes the normal contact force, $E^*$ denotes the equivalent Young's modulus, $R^*$ denotes the equivalent radius, and $k_p$ denotes the coordination number.

According to Equations (1)–(3), the energy input from the disk can be transferred and converted between the moving and static materials through contact if there is no rigid fixed boundary (such as a trough), which is a flexible constraint. Energy can be transferred between all particles in contact with each other. Equations (2) and (3) show that the kinetic and elastic potential energies in a static material change, eventually resulting in changes in the velocity and contact force of the material. When determining the boundary of the finite dissipation zone, the energy transfer between particles decreases, and physical quantities, such as velocity, displacement, and contact force, also inevitably decrease. Therefore, there exists a flexible constraint boundary at a distant location, where the particles are in a limit equilibrium state. The characteristics of the finite dissipation zone can be studied by analyzing the variation laws of the material velocity and contact force of the materials outside the disk diameter.

The DEM uses Newton's second law for each particle in a time step in the calculation domain to obtain the acceleration, velocity, and displacement. Additionally, the DEM requires the parameters of each particle at the subsequent time step. The motion state and position information of all particles within a certain time interval can be obtained by continuously repeating this process for each particle [19,21].

### 2.2. Model Establishment

The DEM simulation was established using EDEM software, which can accurately simulate and analyze the dynamic behavior of bulk materials using the DEM, as shown in Figure 2. The dimensions of the main components are shown in the figure. The diameter of the disk was 30 mm; the size of the case was 52 × 62 × 30 mm.

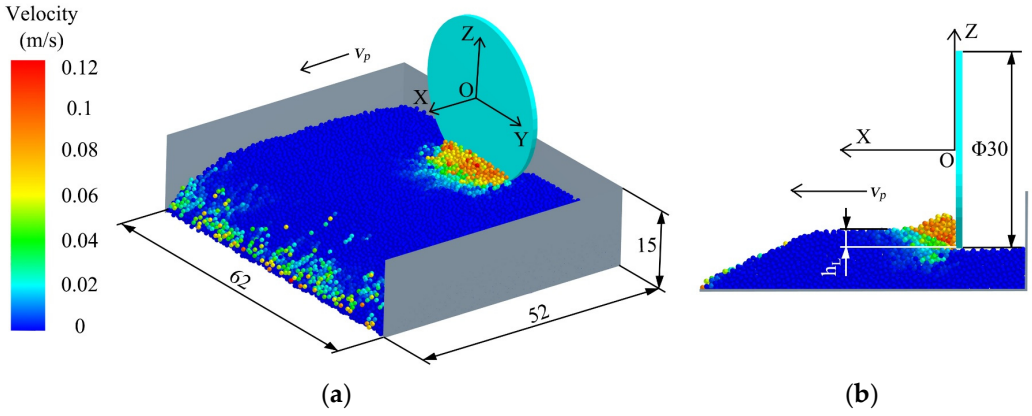


**Figure 2.** Schematic diagram of simulation model. (**a**) axonometric drawing; (**b**) side view.

In the simulation, single spherical particles with diameters of 0.8 mm ± 10% were free-flowing, dry, and non-viscous. The stacking angle was 21.8° and the stacking density was $\rho$ = 709 kg/m$^3$. Using the Hertz–Mindlin no-slip contact model, the time step was 9.8 × 10$^{-6}$ s, and the cell size was 1.2 mm. The data were saved every 0.02 s during the simulation. Movement data, such as displacement, velocity, contact force between particles, and mass flow rate, were obtained after reaching a stable state. The contact characteristics between the disk, particles, and particles in the simulation are listed in Table 1. Using single spherical particles can simplify the computational complexity in a simulation, and compared to multi-spherical particles that are closer to the actual particle shapes, they can also generate similar deformation regions [22].

**Table 1.** Contact characteristics.

| Name of Parameter | Disk | Particles |
|---|---|---|
| Poisson's ratio | 0.3 | 0.4 |
| Shear modulus (Pa) | $1 \times 10^6$ | $2 \times 10^6$ |
| Density (kg/m$^3$) | 7850 | 1200 |
| Collision recovery coefficient (particle–particle) | | 0.5 |
| Static friction coefficient (particle–particle) | | 0.3 |
| Rolling friction coefficient (particle–particle) | | 0.01 |
| Collision recovery coefficient (disk–particle) | | 0.5 |
| Static friction coefficient (disk–particle) | | 0.25 |
| Rolling friction coefficient (disk–particle) | | 0.1 |

First, 10 mm thick materials were placed in the case, and the free surface of the material was horizontal. At this time, the materials flowed out of the case through the discharge port, owing to their weight. Initially, the disk was located at the rear wall of the case, which was 5 mm higher than the material surface. Second, the disk slowly descended into the material to the lowering depth $h_L$. Keeping $h_L$ constant, the disk moved evenly at a translation velocity $v_t$ along the direction perpendicular to the rear wall of the case, until the disk moved out of the case to complete the simulation. Third, the material was discharged from the discharge port through the movement of the disk to achieve the directional flow of the material. Here, $h_L$ = 1.5, 3, and 4.5 mm, and $v_t$ = 30, 45, and 60 mm/s.

The Cartesian coordinate system shown in Figure 2a was established with the disk axis as the X-axis, the horizontal direction as the Y-axis, and the lead hammer as the Z-axis. The zero point of the X-axis was fixed to the bottom surface of the disk and followed the movement of the disk. The direction from the rear wall of the case to the discharge port was in the positive direction of the X-axis. The Y- and Z-axes were zero on the disk axis, and the positive direction of the Z-axis was vertically upward. The positive direction of the Y-axis was determined based on the right-hand Cartesian coordinate system.

In the simulation process, when there is stress concentration in the particle, the particle is broken, causing local instability, and the coordination number also changes so that the force and energy fluctuate. This article mainly focused on the theoretical study of the characteristics of the finite dissipation zone; therefore, it was assumed that the particles do not break during their movement [23,24].

### *2.3. Model Validation*

Gijsen studied the law of material movement driven by a disk, and explored the effects of the slot length, width, and material diameter on the work performed by the disk [25]. He found that the work linearly increased with an increase in the disk's movement by distance, regardless of the changes in the slot length, width, and material diameter. The simulation model used in this study was small. Therefore, the variation rule of disk work over time was derived to verify its correctness, as shown in Figure 3. The input work of the disk increased linearly at different lowering depths with the translation distance, and the trend was the same as that observed by Gijsen. The same material pile appeared on the disk and a shear surface extended obliquely from the lowest point of the disk to the material surface, as shown in Figure 2.

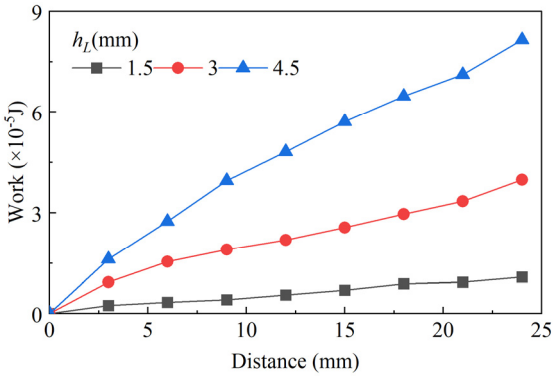


**Figure 3.** Variations in input work with distances at different $h_L$.

The abovementioned phenomenon illustrates the correctness of the simulation model used in this study. Additionally, the data derived demonstrated high reliability for analyzing the material's motion state under the action of the disk.

## 3. Results

The disk promoted the movement of the material within a certain range when it entered the static material and was translated. However, there was no fixed boundary between the moving and static materials. The disk force can overflow through tight contact and compression between the moving and static materials, forming a finite dissipation zone outside the diameter range of the disk. In this section, further research is presented on the properties of the finite dissipation zone.

### *3.1. Mass Flow Rate*

A significant shear plane was generated within the material under the disk that was similar to soil subjected to passive earth pressure under quasi-static conditions, with its direction extending obliquely from the bottom of the disk to the surface of the material, as shown in Figure 4. The material between the shear surface and disk moved at a higher velocity, which was a moving material driven by the disk. The figure clearly shows that the velocity of the material on the shear plane is close to 10 mm/s, not 0 mm/s. Therefore, there must be a velocity transition region outside the shear plane, known as the finite dissipation region. The materials inside were in close contact with each other, and there was a squeezing effect between them. The material particles moved slowly or hardly at all.

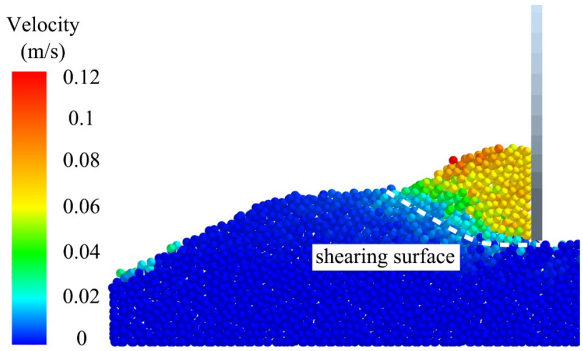


**Figure 4.** Schematic diagram of moving particles in section XZ. The dotted lines indicate the location of the shear plane.

The variation rule of the mass flow rate with time at different $h_L$ and $v_t$ = 60 mm/s is shown in Figure 5. The amount of moving material linearly increased with time, as the disk continued to move. However, the proportion of moving materials between the shear surface and disk at 0.6–0.7 s (i.e., material velocity higher than 10 mm/s) decreased with

time, indicating that the amount of slowly moving materials increased significantly during this period and the overflow of force was considerable. The force of the disk extended to the material at the discharge port after 0.75 s when $h_L$ = 3 and 4.5 mm, which damaged the equilibrium state of the material at the discharge port, caused a large amount of material to flow out owing to its own weight, made the shear plane no longer obvious, and significantly increased the proportion of the moving material. Simultaneously, the effect of force through contact gradually decreased, with an effective action length of 8-times the particle diameter.

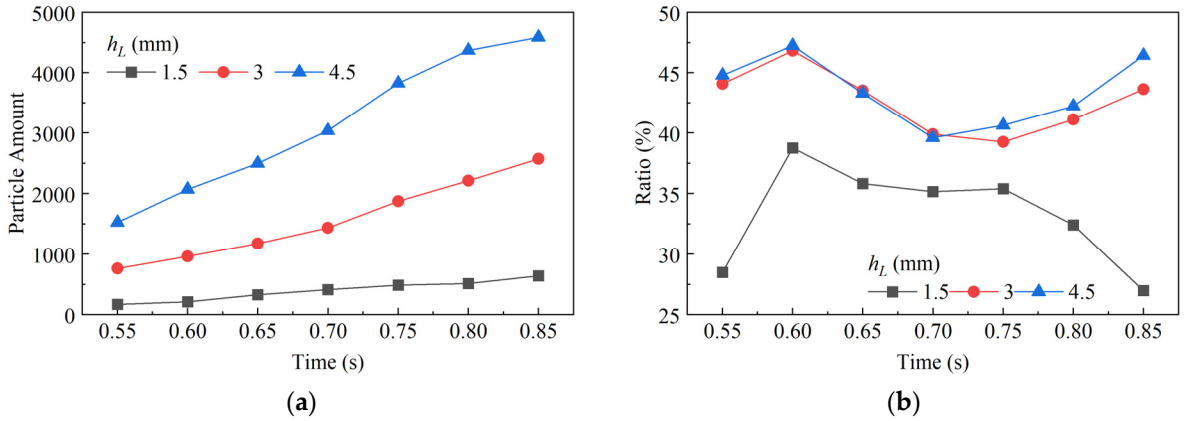


**Figure 5.** Variation rule of the mass flow rate with time at different $h_L$ and $v_t$ = 60 mm/s. (**a**) Amount of the moving material. (**b**) Proportion of material volume with a velocity higher than 10 mm/s within the boundary.

The distances between the section and disk were 0, 3, and 6 mm, as shown in Figure 6a–c, respectively. Only material velocities higher than 1 mm/s are shown in the diagram. Almost all moving materials were within the diameter range of the disk at 0 mm, with velocities close to $v_t$. Additionally, almost no material moved at a low velocity and outside the diameter of the disk, as shown in Figure 6a. The contact force overflowed and the edge curve significantly exceeded the disk diameter after a slight increase in the distance from the disk, as shown in Figure 6b. The distance from the disk continued to increase, as shown in Figure 6c. The edge curve overshoot was similar to that of Figure 6b; however, the amount of material moving at a low velocity increased significantly. At this time, the distance was relatively great and the contact force decreased and transmitted. Therefore, the material could only move at a low velocity. The amount of material moving at a low velocity outside the shear plane increased as the distance increased (i.e., the dark-blue areas in Figure 6b,c increased) and exceeded the disk's diameter. The force and motion of the material near the disk were perpendicular to the disk, and there was almost no overflow due to the disk.

Materials within the diameter range of the disk were subjected to the continuous action of the disk, and moved continuously as the disk moved. Materials outside the boundary generated a certain amount of motion through the friction drive of moving materials. However, their driving force was low and a sustained effect was not created, resulting in energy dissipation. Therefore, the motion state of materials within the finite dissipation zone was studied to determine the location and size of the finite dissipation zone and provide a theoretical basis for efficient directional material flow.

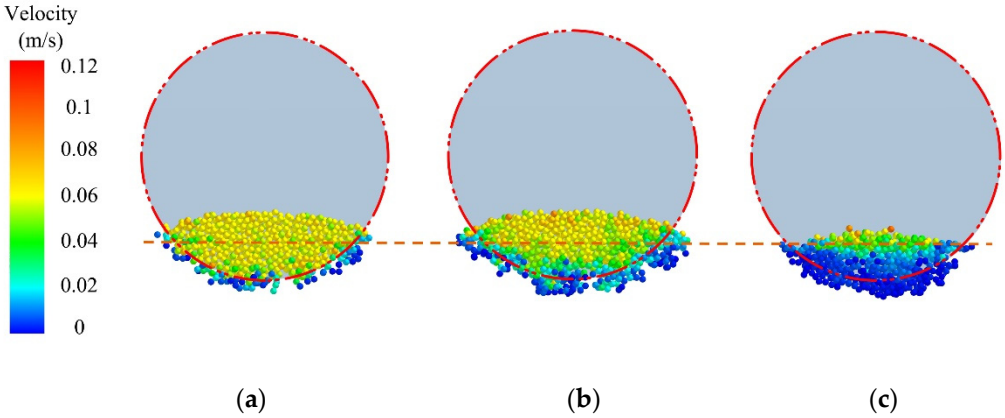


**Figure 6.** Schematic diagram of material velocity within the YZ section at different locations to the disk. The distances between the section and disk are: (**a**) 0, (**b**) 3, and (**c**) 6 mm.

### *3.2. Displacement*

The material in the finite dissipation zone moved at a low velocity, was unable to withstand the continuous force of the disk, and could only move short distances. This was clearly demonstrated by combining the statistical results of Figures 4 and 6, as illustrated in Figure 7. The movement data of materials with a movement distance greater than 0.1 mm (between 0.5–0.8 s) were exported, and the datum with a movement distance of 0.1–1 mm was highlighted. The variation trends of the curves for various $h_L$ values were similar, and the proportion of materials with a moving distance greater than 1 mm was approximately 30%. This indicated that 70% of the moving materials were located in a finite dissipation area. The increase in $h_L$ significantly reduced the proportion of materials with a moving distance of 0.1–0.3 mm from 48.8% to approximately 35%. Additionally, the proportion of materials with a moving distance greater than 1 mm increased to 34%, indicating a decrease in disk force overflow.

A finite dissipation zone surrounded the boundary of the disk and was driven by a moving material with a higher velocity through friction, as observed from the gradual change in the material velocity in Figure 6. Here, the material displacement gradually decreased as the distance from the center of the disk increased. The displacement of the material was 0.3–1 mm, and the proportion of the material with different displacements scarcely changed with $h_L$. This indicated that a stable finite dissipation zone formed outside the disk. The movement distance of the edge material was 0.3 mm, indicating that the average material velocity was 1 mm/s. This velocity can initially be defined as the boundary between the finite dissipation zone and stationary materials.

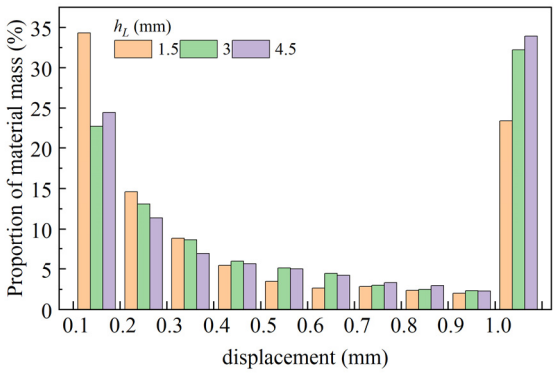


**Figure 7.** Proportion of material displacement under different $h_L$ from 0.5–0.8 s.

### *3.3. Material Velocity and Contact Force*

To verify the accuracy of a finite dissipation zone boundary of 1 mm/s during simulations with $h_L$ = 3 mm and $v_t$ = 60 mm/s, rectangular statistical boxes 1 and 2 with widths of

2 mm were set at distances of 6 and 18 mm from the rear wall of the case, respectively. The XZ section is shown in Figure 8, where the blue, dashed boxes represent the statistical boxes. The laws of material velocity and contact force in the finite dissipation zone (1–10 mm/s) and outside the zone (0.1–1 mm/s) were analyzed using 1 and 10 mm/s as the dividing lines. The disk exceeded boxes 1 and 2 at 0.6 and 0.8 s, respectively.

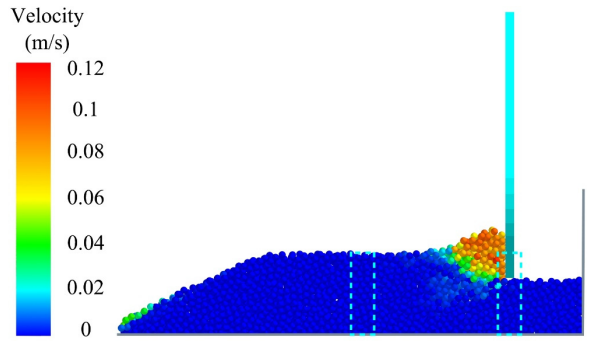


**Figure 8.** Schematic diagram of the location and size of the statistical boxes. The blue, dashed lines indicate the size and location of boxes 1 and 2, which are (from **right** to **left**) 6 and 18 mm away from the rear wall of the case, respectively.

The data from statistical boxes 1 and 2 are shown in Figure 9a,b, respectively. The peak values of the average velocity of materials in the finite dissipation zone for boxes 1 and 2 are clearly shown at approximately 0.6 and 0.8 s, respectively, with peak values of 3.5 mm/s. The velocity curve presented a gradual upward trend as the disk continued to approach the statistical box, between 0.5–0.62 and 0.68–0.79 s. The velocity decreased because there was no further input of disk force after the disk passed the statistical box. Subsequently, the surface materials were restacked under the gravity and the downward trend of velocity decreased, which was demonstrated in two stages at 0.62–0.7 and 0.79–0.86 s. The velocity change curve varied with the distance between the disk position and statistical box, indicating that the energy of material movement in the finite dissipation zone resulted from the disk input. The velocity of the material outside the finite dissipation region fluctuated only slightly as the disk passed. However, its value was only 2.85% of the peak value, which was 0.17% of $v_t$. Using the velocity criterion, the material velocity at the edge of the finite dissipation zone was 1 mm/s.

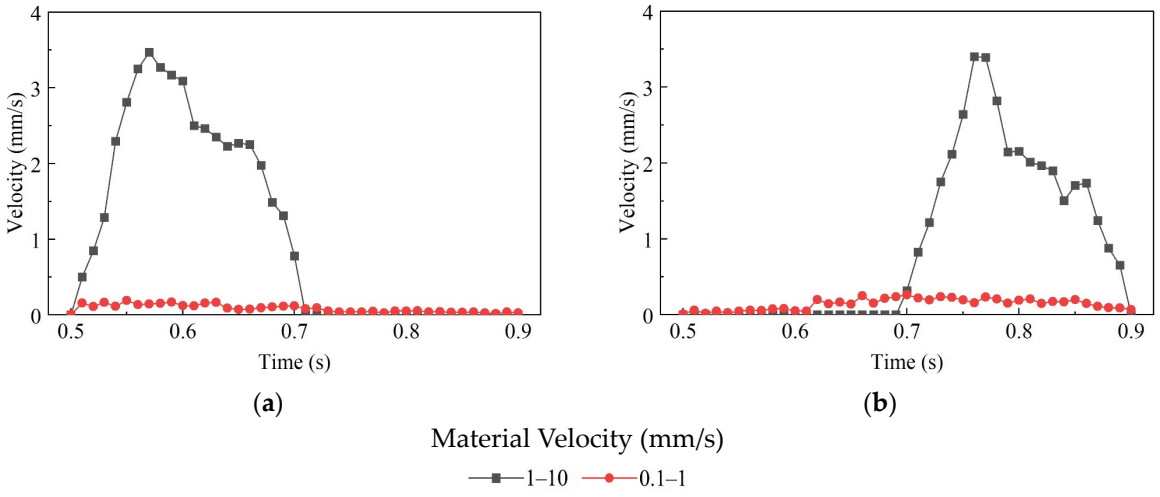


**Figure 9.** Average velocity of the material inside and outside the finite dissipation zone for $h_L$ = 3 mm. Data for statistical boxes: (**a**) 1 and (**b**) 2.

Similar to the velocity curve shown in Figure 9, the average contact force curves of the materials inside and outside the finite dissipation zone followed the same rule. The data from statistical boxes 1 and 2 are shown in Figure 10a,b, respectively. The contact force in the limited dissipation region also varied with the distance between the statistical frame and disk. This indicated that the change in the contact force in materials ranging from 1–10 mm/s was caused by the movement of the disk, which was an overflow of the disk force. However, the peak positions were located at approximately 0.55 and 0.75 s, which were less than 0.6 and 0.8 s, indicating that the finite dissipation zone was not directly below the disk when subjected to the maximum action during the disk's movement. The peaks in Figure 10a,b are $7.4 \times 10^{-4}$ N and $9.5 \times 10^{-4}$ N, respectively. The amount of moving material increased as the disk continued to move, as shown in Figure 5. Additionally, the resistance increased, causing the force transmitted between the particles to significantly increase.

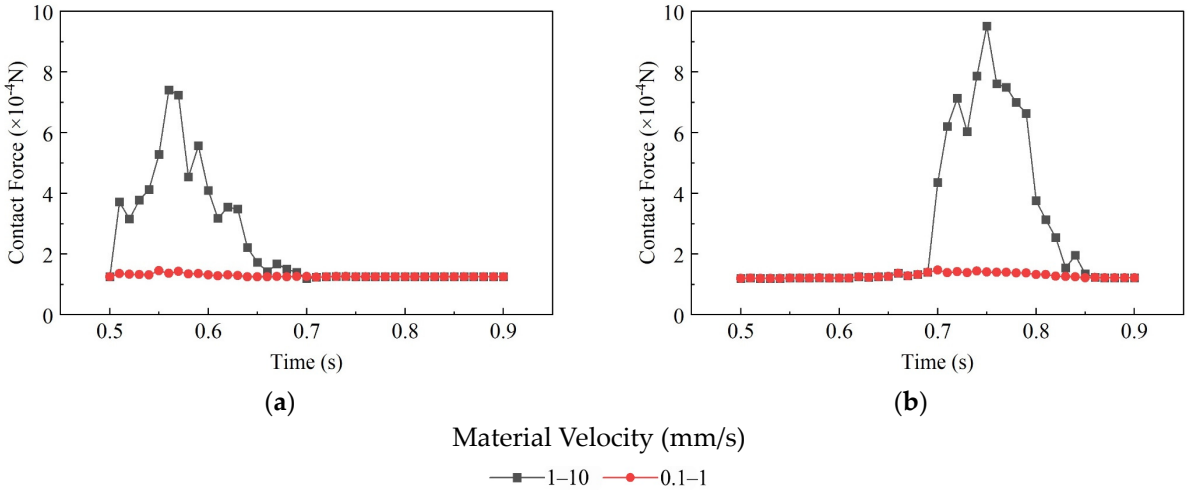


**Figure 10.** Average contact force of the material inside and outside the finite dissipation zone for $h_L$ = 3 mm. Data for statistical boxes: (**a**) 1 and (**b**) 2.

The force of the disk generated an overflow through close contact between the material particles when $v_t$ = 60 mm/s. Based on the data results in Sections 3.2 and 3.3, 1 mm/s was chosen as the boundary of the finite dissipation zone, thereby determining the effective range of action of the disk-force overflow. The variation in size with the operating parameters needs to be explored further.

### *3.4. Edge Curves and Size*

The XZ section for materials with velocities higher than 1 mm/s is shown in Figure 11. The dashed line represents the shear surface and the dotted-dashed line represents a vertical line passing through the intersection point of the shear and static material surfaces. A finite dissipation zone surrounded the shear plane and the velocity of the dark-blue particles was 1 mm/s, forming an edge curve. Considering the inclination of the edge curve on both sides of the dotted line, the finite dissipation can be divided into two parts that are located below and in front of the shear plane. The boundary of the finite dissipation zone below the shear surface first rapidly increased with an increase in the distance from the disk, and then sloped slightly towards the material surface. The edge of the finite dissipation zone in front of the shear plane had a large inclination angle and rapidly extended towards the material surface.

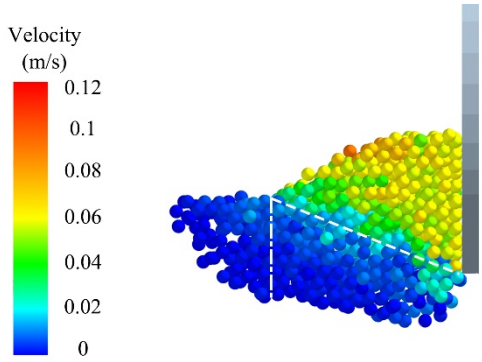


**Figure 11.** Schematic diagram of XZ section for materials with a velocity higher than 1 mm/s.

The material in front of the shear surface also mainly moved at a low velocity, creating boundaries similar to those of the shear surface without significant uplift deformation on the surface. Almost all materials were within the diameter range of the disk from the positive direction of the X-axis, as shown in Figure 12. An effective force was generated as the disk continued to move, resulting in motion.

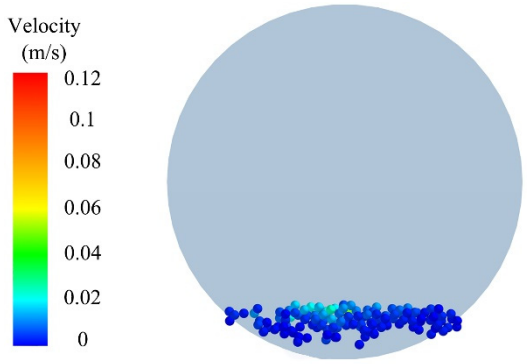


**Figure 12.** YZ section of the materials in front of the shear plane with a velocity higher than 1 mm/s.

Seven rectangular statistical boxes with a thickness of 2 mm were set up in front of the disk along the X-axis to calculate the edge curves at different distances, and the results are shown in Figure 13. Only 0–8 mm data were obtained when $h_L$ = 1.5 mm, owing to the small action area and limited range of the finite dissipation zone. The solid line represents the edge curve of the finite dissipation zone at different distances, the dashed line represents the boundary of the disk, the dotted-dashed line represents the height of the initial surface of the material, and the distance between the dotted-dashed line and the lowest point of the solid line (Z = −15 mm) represents the lowering depth. The edge of the finite dissipation zone formed a set of concentric circular curves with the same center as the disk, as shown in Figure 13. The distance from the disk edge increased slightly, when approaching the material surface. The data from the XZ section were obtained to represent the size of the finite dissipation zone, display the edge position of the finite dissipation zone more intuitively, and because the edge curve of the finite dissipation zone was nearly circular.

The maximum boundary of the finite dissipation zone extended 2.5–3.0 mm outside the disk (approximately 3–4 times the diameter of the particle) when $v_t$ = 60 mm/s, as shown in Figure 14. Additionally, the larger the $h_L$, the larger the extension. When $h_L$ =1.5, 3, and 4.5 mm, the maximum boundaries appeared at X = 2, 3, and 4 mm, respectively. The boundary of the finite dissipation zone first extended downward from X = 0 mm to the maximum boundary, and the included angle with the Z-axis in the vertical plane was 45° ± 4°. This part of the material was subjected to the resistance of the static material in front and the component force of the disk. The material was in a state of two-force equilibrium, which caused damage along the slope owing to compression. The force transmitted between the

materials gradually decreased as the distance from the disk continued to increase, and the boundary of the finite dissipation zone gradually extended towards the surface. It was difficult to form an effective force after crossing the intersection point between the shear and initial material surfaces. Furthermore, the boundary of the finite dissipation zone rapidly extended towards the surface.

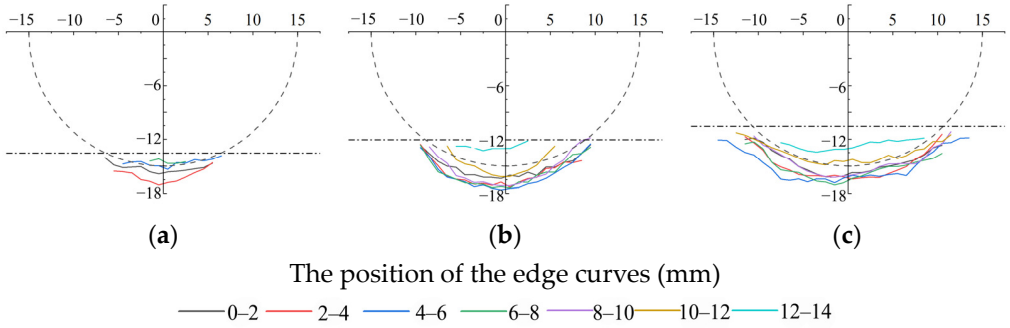


**Figure 13.** Edge curves of finite dissipation regions at different distances at 0.6 s. The descending depths are: (**a**) 1.5, (**b**) 3, and (**c**) 4.5 mm.

The maximum X coordinate of the boundary of the finite dissipation zone was approximately 4–5-times $h_L$, as shown in Figure 14. The curve of 0.8 s slightly increased after X > 4 mm and maintained a depth of −16.6 mm, until it reached the discharge port, without a two-stage transition, as shown in Figure 14c. The main reason for this was that moving materials accumulated more over a long period of time when $h_L$ was deep. In addition, the force was transmitted through contact for long distances. However, the material at the discharge port was already in a balanced state because of its weight. Its balance can be broken when subjected to a small thrust in the X-direction, causing a large amount of material to flow out of the discharge port from the material tank.

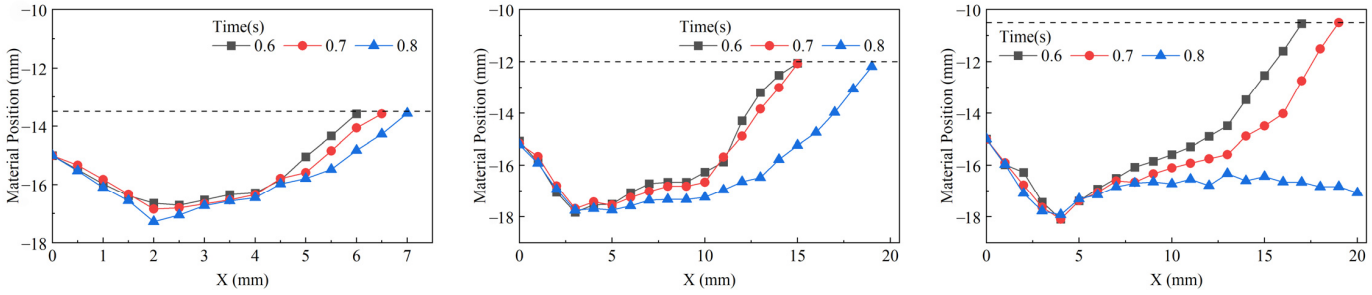


(**a**) $h_L$ = 1.5 mm (**b**) $h_L$ = 3 mm (**c**) $h_L$ = 4.5 mm

**Figure 14.** Edge curves of the finite dissipation zone formed during the transition of disks with different descending depths within 0.6–0.8 s, where $h_L$ equals: (**a**) 1.5, (**b**) 3, and (**c**) 4.5 mm.

### *3.5. Translation Velocity*

Translation velocity $v_t$ is also an important parameter in the disk motion process. Changes in $v_t$ affect the velocity gradient within the moving material, thereby affecting the contact force and characteristics of the finite dissipation zone. In this section, two translational velocities (30 and 45 mm/s) were selected to explore the relevant properties of the finite dissipation zone when $h_L$ = 3 mm.

#### 3.5.1. Material Velocity and Contact Force

First, the applicability of using 1 mm/s as the boundary of the finite dissipation zone for different values of $v_t$ was discussed. The material velocity on the shear surface was approximately 10 mm/s, using the same method as in Section 3.3 and a statistics box at the same location. Subsequently, the change laws of the material velocity and contact force

were calculated. The variation law of the material velocity in the statistical frame at 6 mm is shown in Figure 15.

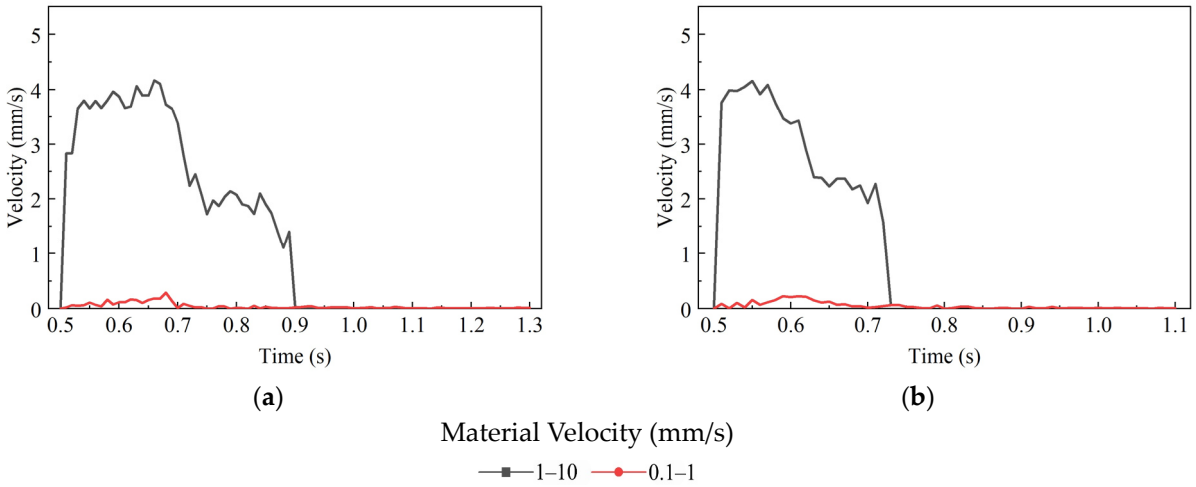


**Figure 15.** Change law of material velocity in the statistical box at the position of 6 mm for $h_L$ = 3 mm, where $v_t$ equals: (**a**) 30 and (**b**) 45 mm/s.

The translational velocities in Figure 15a,b were 30 and 45 mm/s, respectively. Overall, the 1 mm/s boundary between the finite dissipation zone and static material was applicable, and the material velocity of 0.1–1 mm/s remained almost constant at 0 with the movement of the disk. The material velocity curve from 1 to 10 mm/s changed with the position of the disk. Using the velocity criterion, 1 mm/s was used as the boundary of the finite dissipation zone. It took 0.4 and 0.23 s from the beginning of the movement of the material to the end, respectively. Compared to 0.2 s at $v_t$ = 60 mm/s, the movement duration was proportional to $v_t$.

The contact-force maintenance time of the materials at 1–10 mm/s in Figure 16 was approximately 50% that of the velocity curve. Overall, the contact force of 0.1–1 mm/s in the two curves was almost constant with the movement of the disk. The change in the contact force mainly existed in materials with a velocity of 1–10 mm/s. The contact force increased as the disk approached, reaching a peak value. The contact force decreased rapidly and returned to the same value as that in the 0.1–1 mm/s materials, when the disk moved past the statistical box. The contact force criterion indicates that 1 mm/s can be used as the boundary of the finite dissipation zone.

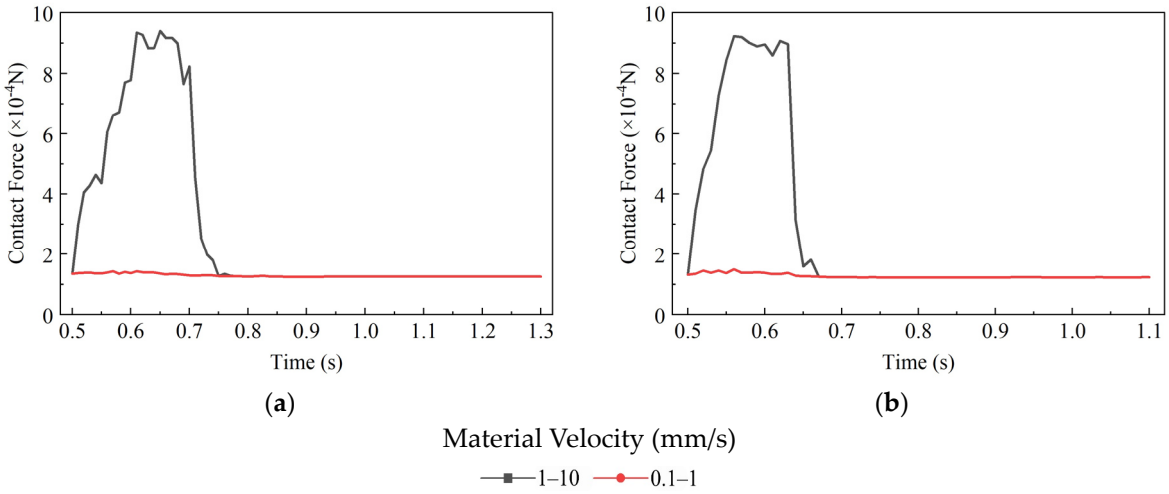


**Figure 16.** Change law of contact velocities in the statistical box at the position of 6 mm for $h_L$ = 3 mm, where $v_t$ equals: (**a**) 30 and (**b**) 45 mm/s.

### 3.5.2. Edge Curves and Size

The XZ section was selected when the disk was moved to the same position under different $v_t$, as shown in Figure 17. Only materials with velocities higher than 1 mm/s are shown in the figure. The velocity of materials on the shear surface was approximately 10 mm/s. The higher the $v_t$, the larger the velocity gradient between the moving materials. In addition, more materials presented a faster motion. The length and diameter of the finite dissipation zone increased with an increase in $v_t$.

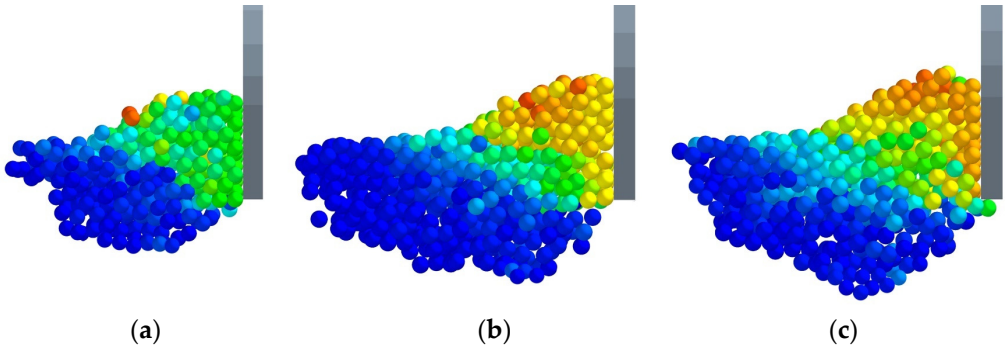


**Figure 17.** Material velocity diagrams of section XZ for materials with a velocity higher than 1 mm/s when the disk is translated to the same position, where $v_t$ equals: (**a**) 30, (**b**) 45 and (**c**) 60 mm/s.

The variation trend of the edge curve of the finite dissipation zone at different $v_t$ values was similar to that of the curve in Figure 13, when $h_L$ = 3 mm and the maximum boundaries are located at X = 3 mm, as shown in Figure 18. However, the maximum boundary of the finite dissipation zone only extended to 0.7 and 1.4 mm outside the disk when $v_t$ = 30 and 45 mm/s, respectively. This was much smaller than the maximum boundary of the finite dissipation zone at 60 mm/s. The angle of the material increased as $v_t$ increased when X = 0–3 mm. Furthermore, the component of the disk overflow force towards the Z-axis decreased. Therefore, reducing $v_t$ effectively reduced the energy dissipation. The angle of the edge curve of the finite dissipation zone from X = 3 mm to the intersection point between the shear and initial material surfaces also increased after $v_t$ decreased. This allowed the finite dissipation zone to rapidly extend to the material surface, thereby reducing the area of the finite dissipation zone and energy consumption.

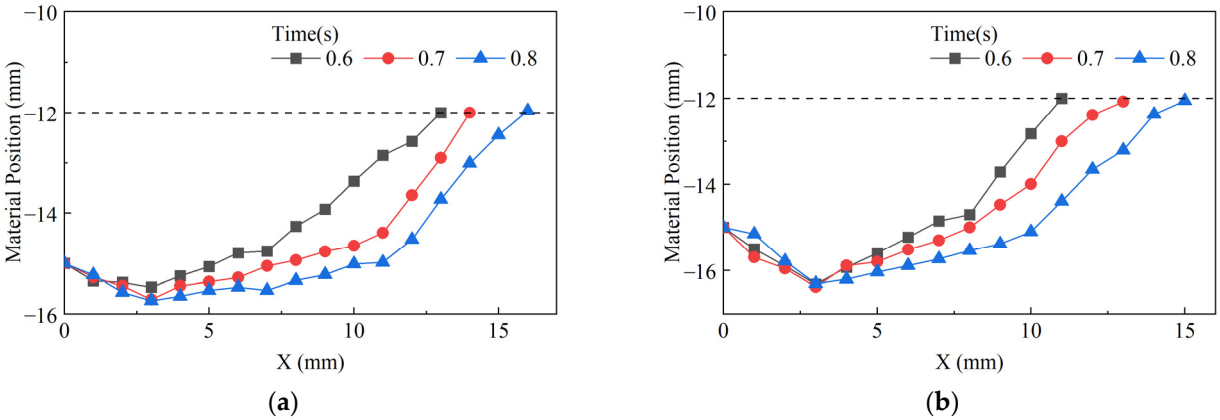


**Figure 18.** Edge curves of the finite dissipation zone at different translational velocities for $h_L$ = 3 mm, where $v_t$ equals: (**a**) 30 and (**b**) 45 mm/s.

The maximum extension distance of the finite dissipation zone at different $v_t$ is represented by the dotted line as a fitting curve for $h_L$ = 3 mm, as shown in Figure 19. In the interval shown in the figure, the maximum extension distance increased linearly with an increase in $v_t$. The boundary of the finite dissipation zone under quasistatic conditions was not applicable to the relevant laws obtained in this study when $v_t$ = 20 mm/s and the maximum extension distance was 0 mm, according to the trend of the fitting curve in the figure.

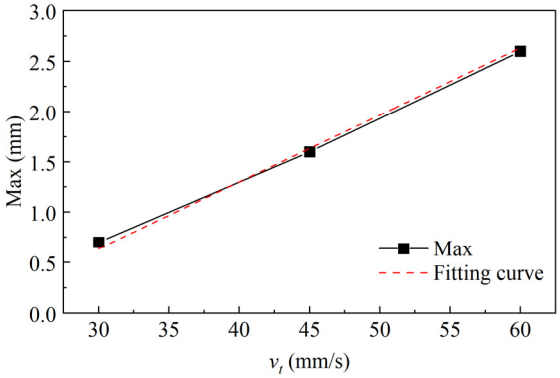


**Figure 19.** Variation in the maximum extension distance of the finite dissipation zone with different $v_t$ for $h_L$ = 3 mm. The dotted line is a fitting curve.

## 4. Discussion

A directional material flow could be formed on the surface of the material under external force excitation. However, the action range extended beyond the physical boundary of the moving component through the strong contact between particles, forming a finite dissipation zone. In this study, a DEM model was established to investigate a finite dissipation zone. The definition, boundary, and characteristics of the finite dissipation zone were studied using criteria, such as material velocity, displacement, and contact force. The main contributions of this study are:

(1) The motion states of all materials in the simulation domain were investigated. An obvious shear surface was also obtained in the directional material flow. However, unlike the shear surface under quasi-static conditions, the material velocity on the shear surface was not zero when the disk moved at a high velocity. There was a transition zone between the shear and wall surfaces of the case, where the material moved at a low velocity. This was defined as a finite dissipation zone.

(2) The displacement, velocity, and contact force of the materials in the finite dissipation zone gradually decreased as the distance from the disk increased. Using these three criteria,

the location of materials at a velocity of 1 mm/s was determined as the boundary of the finite dissipation zone. It was discovered that materials of 0.1–1 mm/s scarcely changed with time, no matter how the disk moved, thereby verifying and determining the boundary of the finite dissipation zone.

(3) The maximum boundary of the finite dissipation zone with different $h_L$ extended between 2.5–3.0 mm outside the disk when $v_t$ = 60 mm/s. The maximum boundary only extended to 0.7 and 1.4 mm outside the disk when $v_t$ = 30 and 45 mm/s, respectively. However, the X-coordinate of the maximum boundary remained almost unchanged, regardless of the $v_t$ changes. The extension distance of the maximum boundary was proportional to $v_t$ when $h_L$ remained the same.

## 5. Conclusions

The movement state, characteristics, and formation mechanism of materials in the zone were studied by establishing a simulation model for the finite dissipation zone. The location of the boundary of the finite dissipation zone was delineated and verified using composite criteria, and the effects of the operating parameters on the finite dissipation zone were obtained. An obvious shear surface was also observed when the disk was translated. However, compared to the quasi-static conditions, low-velocity moving materials surrounded the moving parts outside the shear surface, forming a limited dissipation zone. Some materials in the finite dissipation zone experienced changes in velocity and contact force, only when they were close to moving parts. Moving parts continued to translate and, after a long distance, the material returned to a low-velocity state, dissipating the energy stored inside.

The research on finite dissipation zones can be used to optimize operating parameters, reduce energy and momentum overflow, and achieve efficient and green material flow. Conducting research on the finite dissipation zone and assigning a certain velocity to the moving parts aligns the conclusions with actual working conditions, further enriching the basic theory of directional material flow. To satisfy the demand for high-velocity material flow, the future research should improve the translation velocity and expand the selected material types, select representative materials, and explore the formation and change mechanisms of the limited dissipation zone under different material characteristics to verify the applicability of the research in this paper.

**Author Contributions:** Conceptualization, H.R. and W.M.; Data curation, H.R.; Formal analysis, H.R.; Funding acquisition, W.M. and X.Z.; Investigation, Z.Z.; Methodology, H.R.; Project administration, W.M.; Resources, X.Z.; Software, H.R.; Supervision, H.R.; Validation, H.R., W.M. and X.S.; Visualization, X.S.; Writing—original draft, H.R. and Z.Z.; Writing—review and editing, W.M. and X.S. All authors have read and agreed to the published version of the manuscript.

**Funding:** This research was funded by the National Natural Science Foundation of China, grant number 52075356 and the Science Foundation for Youths of Shanxi Province, grant number 202203021212322.

**Data Availability Statement:** Not applicable.

**Conflicts of Interest:** The authors declare no conflict of interest.

## References

1. Schott, D.L.; van Wijk, L.A.; Vlasblom, W.J. Estimating the homogenization efficiency of mammoth silos by process dynamics and simulations comparing the results of process dynamics with the simulations. *Chem. Eng. Process.* **2005**, *44*, 297–302.
2. Hou, Q.; Dong, K.; Yu, A. DEM study of the flow of cohesive particles in a screw feeder. *Powder Technol.* **2014**, *256*, 529–539. [CrossRef]
3. Badani-Prado, M.A.; Kecojevic, V.; Bogunovic, D. Coal quality management model for dome storage (DS-CQMM). *J. S. Afr. Inst. Min. Metall.* **2016**, *116*, 699–708. [CrossRef]
4. Ren, H.; Meng, W. Discrete numerical simulation of performance analysis of horizontal trough-free screw conveyor in dynamic equilibrium state. *Powder Technol.* **2022**, *407*, 117677. [CrossRef]
5. Ren, H.; Meng, W.; Sun, X.; Zhao, Z.; Zhao, X. Discrete element analysis on dynamic characteristics of directional material flow driven by horizontal trough–free screw conveyor. *Powder Technol.* **2023**, *418*, 118276. [CrossRef]

6. Jarray, A.; Shi, H.; Scheper, B.J.; Habibi, M.; Luding, S. Cohesion-driven mixing and segregation of dry granular media. *Sci. Rep.* **2019**, *9*, 13480. [CrossRef]
7. Karapiperis, K.; Stainier, L.; Ortiz, M.; Andrade, J.E. Data-Driven multiscale modeling in mechanics. *J. Mech. Phys. Solids* **2021**, *147*, 104239. [CrossRef]
8. Shimizu, Y.; Cundall, P.A. Three-dimensional DEM simulations of bulk handling by screw conveyors. *J. Eng. Mech.* **2001**, *127*, 864–872. [CrossRef]
9. Kingston, T.A.; Geick, T.A.; Robinson, T.R.; Heindel, T.J. Characterizing 3D granular flow structures in a double screw mixer using X-ray particle tracking velocimetry. *Powder Technol.* **2015**, *278*, 211–222. [CrossRef]
10. Ruiz-Carcel, C.; Starr, A.; Nsugbe, E. Estimation of powder mass flow rate in a screw feeder using acoustic emissions. *Powder Technol.* **2018**, *336*, 122–130. [CrossRef]
11. González-Montellanon, C.; Ramírez, Á.; Gallego, E. Validation and experimental calibration of 3D discrete element models for the simulation of the discharge flow in silos. *Chem. Eng. Sci.* **2011**, *66*, 5116–5126. [CrossRef]
12. Chen, Y.; Ma, G.; Zhou, W.; Wei, D.; Zhao, Q.; Zou, Y.; Grasselli, G. An enhanced tool for probing the microscopic behavior of granular materials based on X-ray micro-CT and FDEM. *Comput. Geotech.* **2021**, *132*, 103974. [CrossRef]
13. Cleary, P.W. Particulate mixing in a plough share mixer using DEM with realistic shaped particles. *Powder Technol.* **2013**, *248*, 103–120. [CrossRef]
14. Kang, D.H.; Choo, J.; Yun, T.S. Evolution of pore characteristics in the 3D numerical direct shear test. *Comput. Geotech.* **2013**, *49*, 53–61. [CrossRef]
15. Chen, X.; Wang, J. Hybrid discrete-continuum model for granular flow. *Procedia Eng.* **2015**, *102*, 661–667. [CrossRef]
16. Sadek, M.A.; Chen, Y.; Zeng, Z. Draft force prediction for a high-speed disc implement using discrete element modelling. *Biosyst. Eng.* **2021**, *202*, 133–141. [CrossRef]
17. Coetzee, C.; Els, D. Calibration of granular material parameters for DEM modelling and numerical verification by blade–granular material interaction. *J. Terramechanics* **2009**, *46*, 15–26. [CrossRef]
18. Zhang, X.; Dai, D. Exact solutions for Janssen effect of lattice disk packings. *Powder Technol.* **2023**, *420*, 118380. [CrossRef]
19. Liu, G.-Y.; Xu, W.-J.; Zhou, Q. DEM contact model for spherical and polyhedral particles based on energy conservation. *Comput. Geotech.* **2022**, *153*, 105072. [CrossRef]
20. Zhao, Z.; Liu, C.; Brogliato, B. Energy dissipation and dispersion effects in granular media. *Phys. Rev. E* **2008**, *78*, 031307. [CrossRef]
21. Ting, J.M.; Corkum, B.T. Computational laboratory for discrete element geomechanics. *J. Comput. Civ. Eng.* **1992**, *6*, 129–146. [CrossRef]
22. Yin, Z.-Y.; Wang, P.; Zhang, F. Effect of particle shape on the progressive failure of shield tunnel face in granular soils by coupled FDM-DEM method. *Tunn. Undergr. Space Technol.* **2020**, *100*, 103394. [CrossRef]
23. Karatza, Z.; Andò, E.; Papanicolopulos, S.-A.; Viggiani, G.; Ooi, J.Y. Effect of particle morphology and contacts on particle breakage in a granular assembly studied using X-ray tomography. *Granul. Matter* **2019**, *21*, 44. [CrossRef]
24. Wang, P.; Yin, Z.-Y.; Wang, Z.-Y. Micromechanical Investigation of Particle-Size Effect of Granular Materials in Biaxial Test with the Role of Particle Breakage. *J. Eng. Mech.* **2021**, *148*, 04021133. [CrossRef]
25. van Gijsen, E.J.C. Effects of Bulk Solid Materials on the Scraping Operation of Reclaim Screws in a Eurosilo: An Analysis Using the Discrete Element Method. Master's Thesis, Technische Universiteit Delft, Delft, The Netherland, 2022.